CHEMELECTROCHEM
COMMUNICATIONS

ChemPubSoc Europe

DOI: 10.1002/celc.201300229

High-Throughput Mapping of the Electrochemical Properties of (Ni-Fe-Co-Ce)O_x Oxygen-Evolution Catalysts

Joel A. Haber,[a] Chengxiang Xiang,[a] Dan Guevarra,[a] Suho Jung,[a] Jian Jin,[b] and John M. Gregoire*[a]

Discovering improved electrocatalysts is critical for many technologically important processes and for the development of new clean-energy technologies. High-throughput methods for measuring fundamental electrochemical properties are demonstrated through the investigation of oxygen-evolution catalysis by using 665 oxide compositions containing nickel, iron, cobalt, and cerium. The behavior of each composition is characterized in 1.0 M NaOH(aq) by using a scanning drop three-electrode cell to perform chronopotentiometry (CP) and cyclic voltammetry experiments. CP measurements at different current densities identify different composition–performance trends, owing to underlying variations in fundamental electrochemical behavior. We report systematic, coincident, composition-dependent trends in the Tafel slopes and the reversible redox potentials of the catalysts. Applying high-throughput electrochemical methods provides insight into composition–property–performance relationships and motivates new directions for the study of catalyst mechanisms by using informatics and theory.

Discovering improved electrocatalysts for the oxygen evolution reaction (OER) is of great importance for efficient solar-fuel generation, electrowinning of metals, regenerative fuel cells, and recharging metal–air batteries.[1] The slow kinetics of the four-electron OER mechanism requires large overpotentials to drive water oxidation at appreciable current densities.[1a–c] Among the numerous compositions investigated, mixed-metal oxides in the (Ni–Fe)O_x and (Ni–Co)O_x composition spaces are among the most active and most studied OER catalysts.[1b,2] Although this technologically important reaction has been studied for more than 50 years, many of the mechanistic details remain under investigation. Recently, we established high-throughput methods to systematically investigate the performance of pseudoquaternary material libraries as OER electrocatalysts and have reported a new, highly active catalyst composition region in the (Ni-Fe-Co-Ce)O_x composition space.[3c] Our continued investigation of this material system has revealed systematic trends in electrochemical signals, which provides a connection between the previously known Ni–Fe and newly discovered Ni–Co–Ce catalysts.

Recent efforts in the development of high-throughput catalyst screening have produced measurement schemes that rely on an indirect figure of merit (FOM), such as imaging the thermal output of active catalysts, the fluorescence of pH indicators, and the fluorescence of an O_2-sensitive material.[4] These techniques generally produce an empirical, scalar metric of catalytic activity for each library sample, which is used to identify optimal catalysts under particular experimental conditions. To access fundamental electrochemical properties[5] and to characterize catalyst performance beyond an engineering FOM, we developed high-throughput methods for a wide variety of electrochemical experiments.[3] By using these methods, we map composition–property–performance relationships in the (Ni–Fe–Co–Ce)O_x composition space, providing new directions for the study of the OER mechanism with these newly discovered Ce-rich catalysts.

We have previously reported the OER catalyst performance (overpotential at 10 mA cm^{-2}) for 5456 compositions at 3.3 at.% intervals for the entire (Ni–Fe–Co–Ce)O_x composition space.[3c] The most interesting variations in activity lie in a pseudoternary cross-sectional plane containing 665 compositions, as depicted in Figure 1a. These compositions were synthesized on a single glass substrate with a conductive F-doped SnO_2 coating by using inkjet printing of elemental precursor inks; each composition was characterized by using a scanning drop three-electrode cell (SDC), as previously reported[3a,c] (see the Supporting Information). The compositional maps of the electrochemical overpotential, η, for the OER in 1.0 M NaOH(aq) at current densities, J, of 1, 10, and 19 mA cm^{-2} were determined by using chronopotentiometry (CP) measurements (Figure 1). For each current density, well-established performance trends are observed, in which a newly discovered family of catalysts, with approximately 50% Ce, yield the lowest overpotential values at low current densities. The relative performance of these new catalysts compared to the previously known transition-metal-oxide catalysts evolves with increasing current density.

To confirm that different composition regions exhibit unique η–J relationships, select compositions ($Ni_{50}Fe_{30}Co_{17}Ce_3$, $Ni_{40}Fe_{20}Co_{20}Ce_{20}$, and $Ni_{30}Fe_7Co_{20}Ce_{43}$) were synthesized by using the same inkjet-synthesis method onto glassy carbon rotating disc electrodes (RDEs). Figure 2 shows the η–J relation-

[a] Dr. J. A. Haber, Dr. C. Xiang, D. Guevarra, Dr. S. Jung, Dr. J. M. Gregoire
Joint Center for Artificial Photosynthesis
California Institute of Technology
Pasadena, California 91125 (USA)
E-mail: gregoire@caltech.edu

[b] Dr. J. Jin
Engineering Division and Joint Center for Artificial Photosynthesis
Lawrence Berkeley National Laboratory
Berkeley California 94720 (USA)

Supporting Information for this article is available on the WWW under http://dx.doi.org/10.1002/celc.201300229.

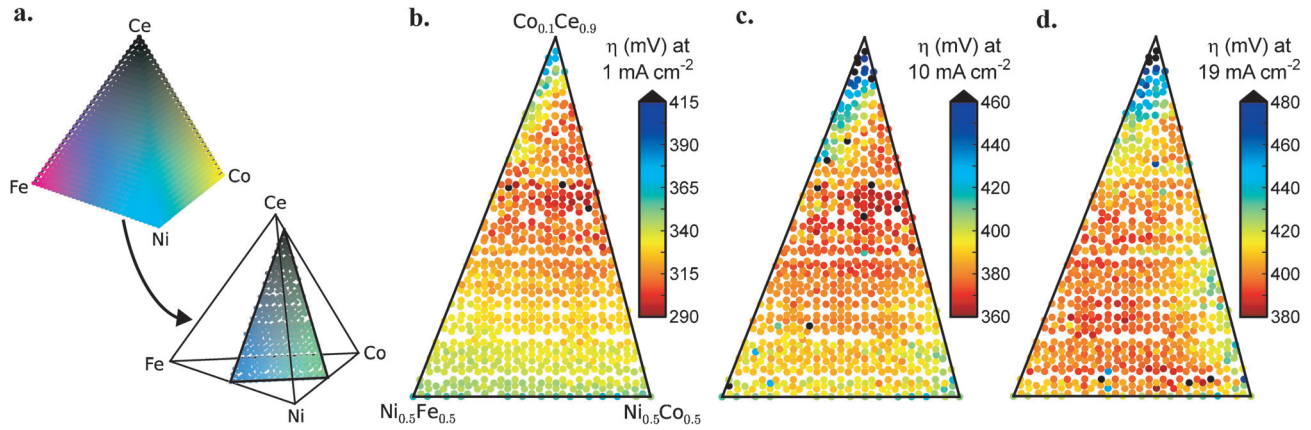

Figure 1. a) Selection of a pseudoternary composition space from the quaternary tetrahedron is shown with compositions colored using the CMYK scheme. For the pseudoternary compositions, the OER overpotential is mapped for b) 1, c) 10, and d) 19 mA cm^{-2}

ships of these RDEs obtained by using standard CP, chronoamperometry (CA), and cyclic voltammetry (CV; 10 mV s^{-1}) in O_2-bubbled 1.0 M NaOH(aq) at 1600 rpm rotation. The exponential relationship between the current and the overpotential, traditionally quantified by the Tafel slope, is consistent in the RDE and SDC data, demonstrating the robust measurement of Tafel slopes though the high-throughput SDC technique. Any discrepancies in the absolute current density between the two measurements are probably caused by the differences in mass transport and the electrochemically accessible surface area.

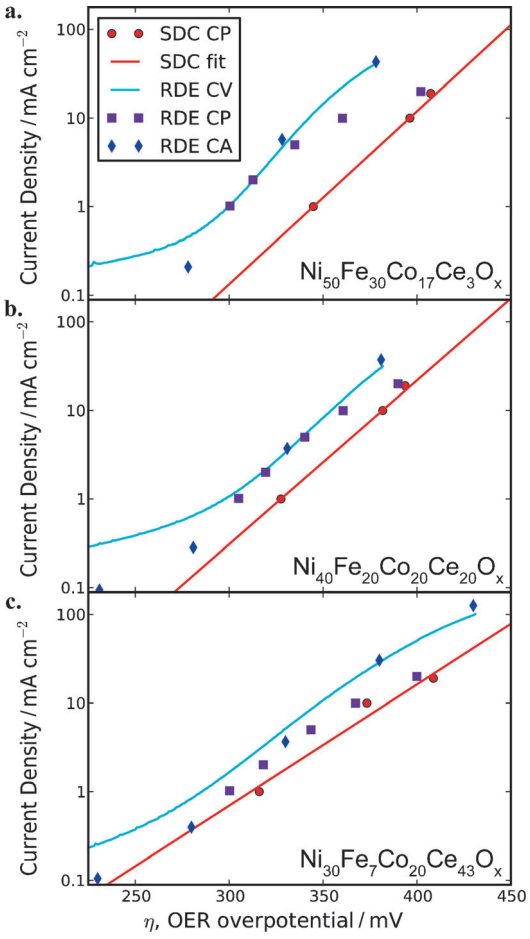

Figure 2. For the three representative compositions, a) $Ni_{50}Fe_{30}Co_{17}Ce_3O_x$, b) $Ni_{40}Fe_{20}co_{20}Ce_{20}O_x$, and c) $Ni_{30}Fe_7Co_{20}Ce_{43}O_x$, the high-throughput SDC CP measurements are shown with a suite of standard RDE measurements. The Tafel slope fit to the SDC CP measurements is also shown.

To visualize the compositional variation of Tafel slopes, a pseudobinary set of compositions were selected from the pseudoternary triangle, as shown in Figure 3a. The pseudobinary line connects two ternary faces of the quaternary space with endpoints of $Ni_{50}Fe_{37}Co_{13}$ from the previously known transition-metal catalyst region and $Ni_{25}Co_{25}Ce_{50}$ from the new Ce-rich catalyst region. The CP results and corresponding Tafel slopes are shown in Figure 3b as a function of composition along this pseudobinary line. The continuously varying Tafel slope describes the performance trend discussed above, most notably that the new $Ni_{25}Co_{25}Ce_{50}$ catalyst region is superior at low current densities and that the optimal composition shifts towards the traditional Fe–Ni region with increasing current density.

The Tafel slope is directly related to the electrochemical reaction mechanism and specifically to the rate-limiting step.[6] However, because multiple reaction mechanisms may be proposed to yield the same Tafel slope, ascribing a particular reaction mechanism based solely upon a measured Tafel slope is controversial.[1a,5a,6,7] Many mechanisms have been proposed and evaluated for the OER;[1a,7,8] however, to our knowledge, no proposed mechanism would produce the Tafel slope of approximately 80 mV per decade, which is observed for the high-Ce catalyst composition (Figure 2c). Moreover, the continuous variation in Tafel slope with composition (Figure 3b) requires a more sophisticated explanation. As explained in the Supporting Information, the variation in Tafel slope from the well-known 45 mV per decade value for Ni–Fe oxides is not solely caused by changes in catalyst resistivity. The observed behavior may result from the shifting importance of two different mechanisms or rate-determining steps with different Tafel slopes, the addition of which produces a continuum shift in effective Tafel slope. Alternatively, the observed behavior could

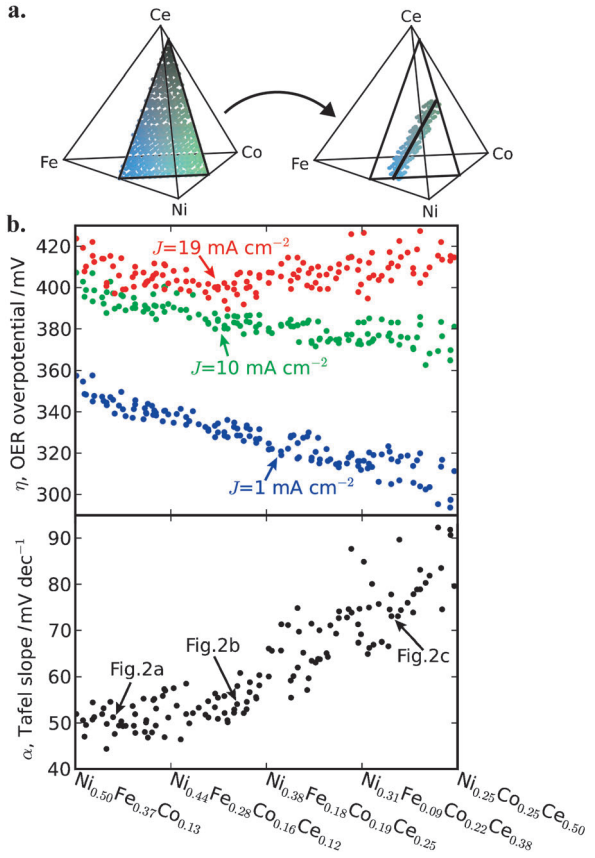

Figure 3. a) The selection of a pseudobinary compositions space from the pseudoternary space of Figure 1 a. b) The SDC CP measurements and derived Tafel slope are shown as a function of pseudobinary composition.

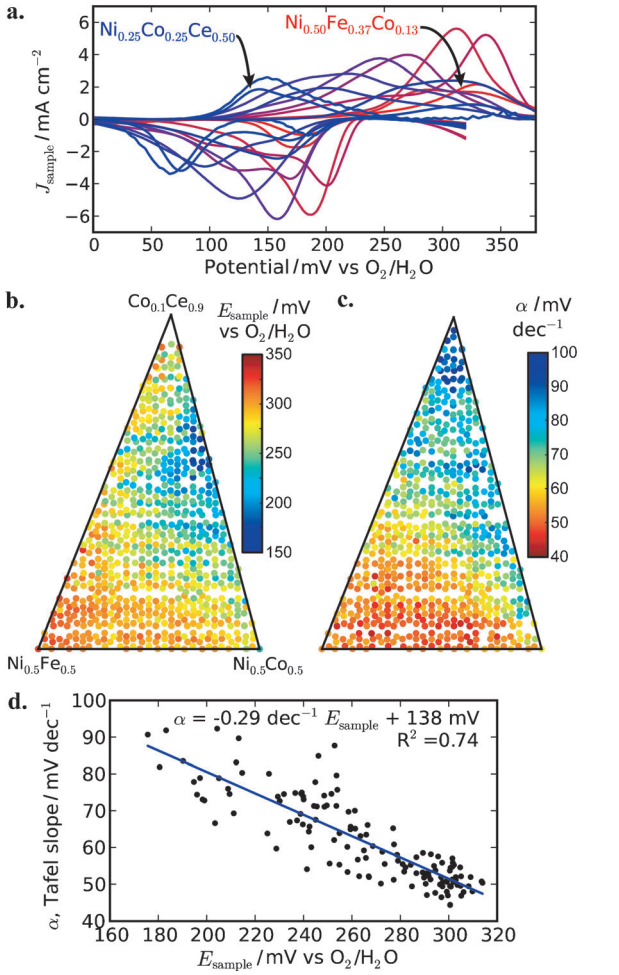

Figure 4. a) The current corresponding to the oxidation and reduction of the catalyst film, as derived from SDC CV measurements for 11 equally spaced compositions on the pseudobinary line of Figure 3 a. b) The pseudoternary map of the average catalyst oxidation potential. c) Map of the Tafel slope from the SDC CP measurements; shown for comparison to the trend in (b). d) By using the pseudobinary compositions from Figure 3, the correlation of the oxidation potential and Tafel slope is demonstrated.

result from a continuous variation in the rate of a process that is Ce-mediated. Ce is well known as an oxygen reservoir in oxidation reactions because of its low redox potential, and is known to be a good oxygen-ion conductor that possessed a high surface-oxygen exchange density at elevated temperatures.[9] The surface-oxygen exchange density and oxygen conductivity are strongly mediated by grain boundaries and segregation of other cations to the grain boundaries.[9d] The catalysts shown in Figure 3 are X-ray amorphous, and further investigation is required to elucidate any relationships among their microstructures, Tafel slopes, and reaction mechanisms.

The discovery of a composition-dependent Tafel slope provides an unprecedented platform for further investigation of catalysis mechanism through material characterization, operando measurements, and theoretical studies. Recent investigations of Ni–Fe OER electrocatalysts has demonstrated that the addition of FeO_x to NiO_x produces an increase not only in catalytic activity but also in the equilibrium potential of the $Ni(OH)_2$/NiOOH redox couple.[2b] To investigate if a similar trend is exhibited in the Ni–Fe–Co–Ce system, a second composition library, with the same compositions described above, was characterized by using CV after a series of CP experiments. As described in the Supporting Information, the η–J data for each leg of CV was modelled to extract the current, J_{sample}, associated with oxidation and reduction of the catalyst. The CV model was found to be robust for $0 < \eta < 380$ mV during the forward sweep and $0 < \eta < 320$ mV for the reverse sweep, as shown in Figure 4 a for 11 equally spaced compositions along the pseudobinary composition line in Figure 3. This series of redox measurements shows a complex but systematic composition dependence of redox behavior. Each J_{sample} signal contains approximately equal and opposite redox charge on the forward and reverse sweeps, indicating that the reactions are reversible. The J_{sample} signals from some composition regions appear to arise from a single redox process, but many compositions produce complex redox signals, apparently arising from multiple, poorly resolved redox processes.

Although additional modeling is required to provide a detailed understanding of these oxidation and reduction waves, for the present report, we extract a simple scalar descriptor for each composition. By using the forward sweep portion of

J_{sample}, the average sample oxidation potential is calculated according to Equation (1):

$$E_{sample} = \int_{0mV}^{380mV} \eta J_{sample} d\eta \Big/ \int_{0mV}^{380mV} J_{sample} d\eta \quad (1)$$

For a single oxidation process E_{sample} is equivalent to the potential of the peak current that is typically used in electrochemical analysis, and, for a multiprocess signal, it is the current (or charge)-weighted average potential of the oxidation peaks. The pseudoternary map of E_{sample} is shown in Figure 4b, and the corresponding map of the Tafel slope is shown in Figure 4c. The striking similarity of the composition maps of E_{sample} and Tafel slope is quantified by using the pseudobinary compositions (Figure 4d). The statistical correlation of the two fundamental electrochemical properties investigated herein may be simply attributed to independent relationships with the underlying composition. However, this correlation motivates the investigation into a link between the energetics of the oxidation of a catalyst and its OER catalysis. The linear correlation suggests that metal oxides that undergo redox transitions closer to the reversible potential for oxygen evolution exhibit higher Tafel slopes. Although oxidation of metal oxides prior to their OER catalysis has been observed in many studies, only a few reports discuss the influence of the oxidation peak position on the kinetics of the water oxidation by using engineering FOMs. Hickling and Hill reported a linear correlation between the OER overpotential at high current density (1 A cm^{-2}) and the redox potential of the catalyst for ten metal anodes.[10] Rasiyah and Tseung extended the study to six different metal oxides and observed a similar correlation between the onset potential of oxygen evolution and the redox potential of the electrocatalysts.[11] During the studies of homogeneous catalysis for CO_2 reduction and oxygen reduction reactions, a strong correlation between the redox potential of the molecular catalyst and the electrocatalytic current was also observed.[12]

Although the focus of this communication is high-throughput mapping of fundamental electrochemical parameters in composition space, we note that Figures 3 and 4 represent important implications for engineering of catalyst electrodes. The Tafel slope indicates the decrease in overpotential that can be attained by increasing the electrochemically active surface area. For a given OER current density, engineering a higher catalyst surface area will produce a significant decrease in overpotential for the high-Ce catalyst compared to the low-Ce catalyst. If catalyst oxidation is a prerequisite for catalytic activity, decreases in operational overpotential are limited by the redox potential of the pertinent catalyst redox couple. Figure 4a shows that, for the $Ni_{25}Co_{25}Ce_{50}$ catalyst region, this reversible redox potential is near an overpotential of 110 mV. The challenge to materials engineers is to fabricate catalyst electrodes that produce technologically relevant current densities at an overpotential approaching this very low limiting value.

The high-throughput, high-fidelity electrochemical characterization employed in this study provides detailed information, both with respect to compositional trends and to property-performance relationships. The ability to generate extensive, high-quality electrochemical data as a function of composition and processing conditions sets the stage for a new paradigm in materials-science research. These capabilities provide new research directions for catalyst discovery and development, and require that models of reaction mechanisms explain continuum behavior changes across complex composition spaces.

Acknowledgements

This manuscript is based upon work performed by the Joint Center for Artificial Photosynthesis, an Energy Innovation Hub, supported through the Office of Science of the U.S. Department of Energy (Award No. DE-SC0004993). The authors thank Dr. Charles McCrory for assistance with RDE experiments, and Drs. Manuel Soriaga, Alexis T. Bell, Mary Louie, and Yun Cai for helpful discussions.

Keywords: combinatorial chemistry · electrochemistry · heterogeneous catalysis · oxygen evolution reaction · solar fuels

[1] a) M. G. Walter, E. L. Warren, J. R. McKone, S. W. Boettcher, Q. X. Mi, E. A. Santori, N. S. Lewis, *Chem. Rev.* **2010**, *110*, 6446–6473; b) T. R. Cook, D. K. Dogutan, S. Y. Reece, Y. Surendranath, T. S. Teets, D. G. Nocera, *Chem. Rev.* **2010**, *110*, 6474–6502; c) M. E. G. Lyons, R. L. Doyle, M. P. Brandon, *Phys. Chem. Chem. Phys.* **2011**, *13*, 21530–21551; d) K. S. Joya, Y. F. Joya, K. Ocakoglu, R. van de Krol, *Angew. Chem. Int. Ed.* **2013**, *52*, 10426–10437.

[2] a) L. Trotochaud, J. K. Ranney, K. N. Williams, S. W. Boettcher, *J. Am. Chem. Soc.* **2012**, *134*, 17253–17261; b) M. W. Louie, A. T. Bell, *J. Am. Chem. Soc.* **2013**, *135*, 12329–12337; c) D. A. Corrigan, *J. Electrochem. Soc.* **1987**, *134*, 377–384; d) I. Nikolov, R. Darkaoui, E. Zhecheva, R. Stoyanova, N. Dimitrov, T. Vitanov, *J. Electroanal. Chem.* **1997**, *429*, 157–168; e) E. B. Castro, C. A. Gervasi, *Int. J. Hydrogen Energy* **2000**, *25*, 1163–1170; f) E. B. Castro, S. G. Real, L. F. P. Dick, *Int. J. Hydrogen Energy* **2004**, *29*, 255–261; g) S. K. Tiwari, S. Samuel, R. N. Singh, G. Poillerat, J. F. Koenig, P. Chartier, *Int. J. Hydrogen Energy* **1995**, *20*, 9–15; h) C. Bocca, A. Barbucci, M. Delucchi, G. Cerisola, *Int. J. Hydrogen Energy* **1999**, *24*, 21–26; i) R. D. L. Smith, M. S. Prevot, R. D. Fagan, Z. P. Zhang, P. A. Sedach, M. K. J. Siu, S. Trudel, C. P. Berlinguette, *Science* **2013**, *340*, 60–63; j) R. D. L. Smith, M. S. Prévot, R. D. Fagan, S. Trudel, C. P. Berlinguette, *J. Am. Chem. Soc.* **2013**, *135*, 11580–11586.

[3] a) J. M. Gregoire, C. X. Xiang, X. N. Liu, M. Marcin, J. Jin, *Rev. Sci. Instrum.* **2013**, *84*, 024102; b) J. M. Gregoire, C. Xiang, S. Mitrovic, X. Liu, M. Marcin, E. W. Cornell, J. Fan, J. Jin, *J. Electrochem. Soc.* **2013**, *160*, F337-F342; c) J. A. Haber, Y. Cai, S. Jung, C. Xiang, S. Mitrovic, J. Jin, A. T. Bell, J. M. Gregoire, unpublished results.

[4] a) A. G. Dokoutchaev, F. Abdelrazzaq, M. E. Thompson, J. Willson, C. Chang, A. Bocarsly, *Chem. Mater.* **2002**, *14*, 3343–3348; b) J. J. Hanak, *J. Mater. Sci.* **1970**, *5*, 964; c) F. C. Moates, M. Somani, J. Annamalai, J. T. Richardson, D. Luss, R. C. Willson, *Ind. Eng. Chem. Res.* **1996**, *35*, 4801–4803; d) E. Reddington, A. Sapienza, B. Gurau, R. Viswanathan, S. Sarangapani, E. S. Smotkin, T. E. Mallouk, *Science* **1998**, *280*, 1735–1737; e) S. J. Taylor, J. P. Morken, *Science* **1998**, *280*, 267–270; f) J. B. Gerken, J. Y. C. Chen, R. C. Masse, A. B. Powell, S. S. Stahl, *Angew. Chem.* **2012**, *124*, 6780–6784; *Angew. Chem. Int. Ed.* **2012**, *51*, 6676–6680.

[5] a) J. O. Bockris, T. Otagawa, *J. Phys. Chem.* **1983**, *87*, 2960–2971; b) S. Trasatti, *Electrochim. Acta* **1984**, *29*, 1503–1512.

[6] A. J. Bard, L. R. Faulkner, *Electrochemical Methods, 2nd ed.*, Wiley, New York **2001**.

[7] J. O. Bockris, *J. Chem. Phys.* **1956**, *24*, 817–827.

[8] a) A. G. C. Kobussen, G. H. J. Broers, *J. Electroanal. Chem.* **1981**, *126*, 221–240; b) L. Formaro, M. Longhi, *J. Phys. Chem. B* **2003**, *107*, 6425–6430.

[9] a) G. S. Zafiris, R. J. Gorte, *J. Catal.* **1993**, *139*, 561–567; b) A. Trovarelli, *Catal. Rev. Sci. Eng.* **1996**, *38*, 439–520; c) M. Cargnello, V. V. Doan-

Nguyen, T. R. Gordon, R. E. Diaz, E. A. Stach, R. J. Gorte, P. Fornasiero, C. B. Murray, *Science* **2013**, *341*, 771 – 773; d) W. Lee, H. J. Jung, M. H. Lee, Y. B. Kim, J. S. Park, R. Sinclair, F. B. Prinz, *Adv. Funct. Mater.* **2012**, *22*, 965 – 971.
[10] A. Hickling, S. Hill, *Discuss. Faraday Soc.* **1947**, *1*, 236 – 246.
[11] P. Rasiyah, A. C. C. Tseung, *J. Electrochem. Soc.* **1984**, *131*, 803 – 808.
[12] a) P. R. Bernatis, A. Miedaner, R. C. Haltiwanger, D. L. Dubois, *Organometallics* **1994**, *13*, 4835 – 4843; b) C. C. L. McCrory, X. Ottenwaelder, T. D. P. Stack, C. E. D. Chidsey, *J. Phys. Chem. A* **2007**, *111*, 12641 – 12650.

Received: November 18, 2013
Published online on December 13, 2013